Influence of graphene oxide on the properties of composite polyacrylonitrile membranes

Beata Fryczkowska*, Dorota Biniaś, Czesław Ślusarczyk, Janusz Fabia, Jarosław Janicki

Faculty of Materials, Civil and Environmental Engineering, Institute of Textile Engineering and Polymer Materials,
University of Bielsko-Biala, Willowa 2, 43-309 Bielsko-Biala, Poland, emails: bfryczkowska@ath.bielsko.pl (B. Fryczkowska),
dbinias@ath.bielsko.pl (D. Biniaś), cslusarczyk@ath.bielsko.pl (C. Ślusarczyk), jfabia@ath.bielsko.pl (J. Fabia),
jjanicki@ath.bielsko.pl (J. Janicki)

ABSTRACT

This paper presents the results of research on the synthesis of graphene oxide/polyacrylonitrile (GO/PAN) composite membranes from *N,N*-dimethylformamide solution using a phase inversion method. Our studies have shown that the presence of GO has a significant effect on the physical and chemical properties of the composite material, which is also confirmed by scanning electron microscopy. In addition, GO has been found to improve the transport properties and prevent fouling behavior. Qualitative studies of the composition of the membranes using an attenuated total reflectance Fourier transform infrared spectroscopy technique proved the presence of GO on the surface of the GO/PAN membrane and, simultaneously, the lack of bands characteristic for PAN, which may explain the phenomena occurring during the transport of liquid through GO/PAN membranes. Thermal analysis (differential scanning calorimetery) confirmed that when graphene oxide is incorporated into the polymer matrix at a level of at least 4%, the properties of the GO/PAN composites are distinctly changed, and the PAN cyclization temperature is much lower. Wide-angle X-ray scattering patterns, on the other hand, showed good dispersion of GO in the composite membranes.

Keywords: Graphene oxide; Polyacrylonitrile; Membranes; Transport properties; $FeCl_3$ rejection

1. Introduction

Polyacrylonitrile (PAN) is a popular engineering polymer that can be obtained in the form of either a homopolymer or a copolymer [1]. The oldest and most well-known application of PAN is in the textile industry, but it also has been used in special textiles [2], carbon fibers [3], antibacterial products [4], superhydrophobic surface finishes [5], optoelectronic and photonic devices [6], energy storage systems [7] and many others. PAN has good thermal stability [8], mechanical properties, thermal conductivity, and UV and chemical resistance [9]. PAN is soluble in many solvents including *N,N*-dimethylformamide (DMF), dimethylsulfoxide (DMSO), *N,N*-dimethylacetamide (DMA), chloroacetonitrile, dioxanone, dimethyl phosphite, dimethyl sulfone, γ-butyrolactone, ethylene carbonate, nitric acid, sulfuric acid, and therefore, it can be easily processed from solution [9–11]. This good solubility allows the preparation of membranes for ultrafiltration (UF), nanofiltration, reverse osmosis and pervaporation [12–15]. One membrane preparation method is phase inversion. The morphology of membranes obtained by this technique, and thus their properties, are influenced by several factors, especially polymer concentration, solvent and coagulant used, and solvent evaporation time [14,16–18]. PAN can also be modified to increase the hydrophobic properties of the initially hydrophilic polymer. Physical techniques for such modification may include plasma treatment [12,19], while the chemical hydrophobization of the PAN surface can be performed using, for example, sodium hydroxide [20–23].

* Corresponding author.

Another way to modify the membrane properties is to form composite materials by incorporating particles of another substance. For polymers, nanoparticles, both inorganic and organic, may be used as such additives. Among the varieties of allotropic carbon that can be introduced into such polymer composites, fullerenes, carbon nanotubes, graphene and graphene oxide have recently received the most attention.

Graphene oxide (GO; Fig. 1) can be prepared through the oxidation of graphite by various techniques [24,25]. The growing interest in GO stems from its excellent sorption properties for numerous metal ions, such as Co(II), Cu(II), Zn(II), Cd(II), Ni(II), As(III), As(V), Pb(II), Au(III), Eu(III) and U(VI) [26]. In addition, GO possesses many different oxygen-containing functional groups [27], such as epoxy, hydroxyl, carbonyl, and carboxyl, which grant hydrophilic properties to GO and makes it easy to form stable aqueous GO dispersions [28,29]. GO may also be dispersed in organic solvents, for example, DMF, *N*-methyl-2-pyrrolidone (NMP), tetrahydrofuran, and ethylene glycol [30]. The presence of numerous functional groups makes GO relatively easy to react with. Lee et al. [31] studied the impact of GO on the cyclization of PAN in a GO/PAN composite and demonstrated that the presence of oxygen groups in GO facilitates the polymer cyclization by lowering the temperature of the process. Other researchers observed the effect of the presence of GO in PAN composites on the formation mechanism of highly porous carbon fibers, which can be used as electrodes in double layer capacitors [32].

GO can also be used to form membranes together with other carbon allotropes such as carbon nanotubes [33–36] or graphene [37–39]. It can be shaped into thin monolayer films [40–43], which may be used for water desalting and purification [37,38,44,45] as well as for membrane distillation [46]. To prepare membranes containing GO, various polymers are used, such as cellulose [47], polyvinylidene fluoride [48,49], polyamide [40,43], polyester [46], polysulfone [41,50,51], polyetherosulfone [42,52] and, PAN. Membranes with added GO may be obtained through a variety of methods, including vacuum filtration [20,53], layer-by-layer deposition [21,54], spin coating [55,56], and drop casting [57].

Cao et al. [55] used a commercial PAN membrane as a substrate for electrospinning a sodium alginate solution containing GO to obtain layered membranes. Hung et al. [20] formed layered PAN membranes by using a phase inversion method,
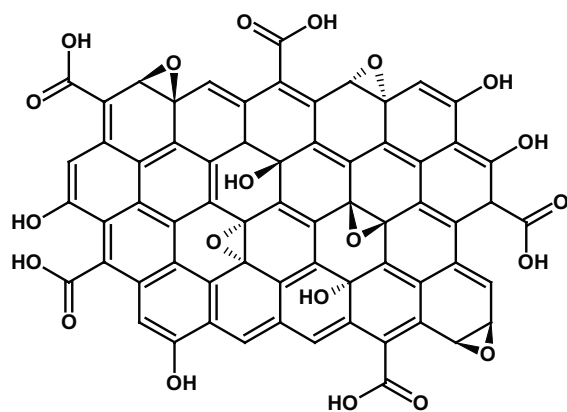
starting from a solution of PAN in NMP that was then used to coat a membrane of polyester nanofibres, which coagulated in water and were treated under vacuum. Uddin et al. [58] prepared GO/PAN membranes from a solution of polyacrylonitrile in DMF, which was mixed with GO dispersed in polyvinyl phenol and then poured and dried to obtain a film. The "layer-by-layer" method with partial hydrolysis of PAN was described by Hu et al. [21]. Initially, they obtained a membrane from PAN/DMF solution using a phase inversion method and then modified the membrane chemically with NaOH. The modified membrane was immersed in a polyelectrolyte solution (poly(allylamine hydrochloride)) and then in dispersed GO. The process was repeated several times, yielding a multi-layer coating of polyacrylonitrile membrane. Zhu et al. [59] prepared GO/PAN membranes by electrospinning from GO/PAN/DMF solution, while Zhang et al. [60] obtained nanofibres from a solution of PAN in DMF and then chemically modified the fiber surfaces using diethylenetriamine (DETA). Then, on the thus-prepared PAN surface, a nano-nonwoven GO dispersion was applied in a highly acidic environment, followed by the chemical reaction between GO and PAN. A multi-component PAN/EtOH/LiCl/DMF solution was proposed by Shen et al. [61] for membrane formation by phase inversion and subsequent treatment with a solution of NaOH. The thus-prepared membranes were coated with an aqueous solution of GO and *m*-phenylenediamine (MPD) and then with a solution of 1,3,5-benzenetricarbonyl trichloride (TMC) in hexane. Under these conditions, an interfacial polymerization reaction occurred, and a thin selective layer of the membrane was created.

A simple technique for the preparation of GO-containing composite membranes is the phase inversion of polymeric blends, instead of coating of the polymer carriers with a GO layer. This paper presents the results of previously unreported studies on GO/PAN composite membrane formation from a homogeneous dispersion of nanosized GO additive in the polymer solution as well as the effect of adding GO nanoparticles on the structural, physicochemical and transport properties as well as the morphology of the PAN membranes. First, GO was synthesized using the modified Hummers' method [62] and dispersed in DMF. Then, PAN was introduced to the prepared dispersion. The solution preparation procedures are similar to those in Zhu et al. [59], but this paper reports different concentrations of GO. From the resulting solutions, polymer films were formed and coagulated in water. In addition, this study presents previously unreported research on the effect of the presence of Fe^{3+} on the transport properties of composite membranes containing GO.

2. Experimental

2.1. Materials

PAN (M_w = 85,000) – copolymer (93.9% acrylonitrile/5.8% methyl acrylate/0.3% methallyl sulfonate) was purchased from Goodfellow Cambridge Ltd., England. Graphite powder <20 μm was purchased from Sigma-Aldrich, Poland. $NaNO_3$, min. 95% H_2SO_4, $KMnO_4$, 30% H_2O_2, DMF, and anhydrous $FeCl_3$ were purchased from Avantor Performance Materials Poland S.A.

Fig. 1. The chemical structure of graphene oxide.

2.2. Synthesis of GO

GO was synthesized according to a modified Hummers' method [62] as described in our earlier work [49]. In brief, 1 g of NaNO$_3$, 46 mL of H$_2$SO$_4$, and 2 g of graphite powder were placed in a flask in an ice bath. After stirring for 30 min, 6 g of KMnO$_4$ was added in small portions so that the temperature of the mixture did not exceed 20°C. After adding all KMnO$_4$ and waiting for 5 min, the mixture was heated to 35°C and stirred at this temperature for 4 h. Then, 92 mL of distilled water was carefully added in portions. Finally, the unreacted KMnO$_4$ was removed. For this purpose, 80 mL of distilled water at 60°C and 50 mL of 3% H$_2$O$_2$ were added. The obtained GO was centrifuged and washed several times with distilled water until the wash water reached pH 7. Wet GO was dried in an oven at 60°C, turning into a brown solid. The resulting GO powder was dispersed in DMF using an ultrasonic bath to prepare the 3.7% w/w GO/DMF dispersion.

2.3. Membrane formation

2.3.1. Forming PAN membranes

PAN membranes were obtained using a phase inversion method. First, a 12% w/w PAN solution in DMF was prepared. The polymer was dissolved at 50°C and then cooled to room temperature (Zhang et al. [63] used a PAN solution at a higher temperature.) The PAN solution was poured onto a clean glass plate and spread using an applicator with a gap width of 0.2 mm [20] or 0.3 mm [49]. Finally, the polymer film was rapidly coagulated in distilled water at room temperature until the membrane detached from the glass. The precipitated membranes ("0" membrane) were air-dried by interposing a layer of tissue paper. To prevent the membrane wrinkling, we used a glass plate load [64].

2.3.2. Forming GO/PAN membranes

PAN solutions (12% w/w in DMF) containing 0.1, 0.5 or 1.0 g of dispersed GO were prepared. To this end, appropriate amounts of 3.7% w/w GO/DMF dispersion were batched and added to a fresh portion of solvent (Table 1) and mixed thoroughly. Then, 12 g of PAN was added and stirred at 50°C. After complete polymer dissolution, the solution was cooled to room temperature. Just before the formation of the membrane, the GO/PAN solution was briefly sonicated, repeatedly

exchanging the distilled water in the ultrasonic cleaner. The well-dispersed GO/PAN solution was then poured onto a clean glass plate and spread using an applicator with a gap width of 0.2 mm [20] or 0.3 mm [49]. Finally, it was rapidly coagulated in distilled water at room temperature until the membrane detached from the glass. The formed membranes were air-dried by interposing a layer of tissue paper and then loaded with the glass plate.

2.4. General characterization

The thickness (l) of the membranes was measured with an Elmetron MG-1 thickness gauge. Samples with dimensions of 1 × 1 cm were weighed using a Sartorius CP224S-0CE analytical balance with an accuracy of 0.0001 g.

The mass per unit area (W_s, g/cm^2) and the density (d_m, g/cm^3) of the membranes were calculated using the following equations:

$$W_s = \frac{w}{s} \tag{1}$$

$$d_m = \frac{w}{s \times l} \tag{2}$$

where w is the mass of a membrane with an area of 1 cm^2, s is the membrane surface area (cm^2), and l is the membrane thickness (cm).

The sorption of water (U) was measured as follows: dry membrane samples (W_d) with dimensions of 1 × 1 cm were weighed on an analytical balance with an accuracy of 0.0001 g and then immersed in distilled water for 10 s. The membranes were then blotted on filter paper and weighed again in the wet state (W_w). The sorption of water was calculated according to Eq. (3):

$$U = \frac{W_w - W_d}{W_d} \times 100\% \tag{3}$$

The porosity of the membranes (ε), which is defined as the ratio of pore volume to the volume of the membrane, was calculated using the following equation [46]:

$$\varepsilon = \frac{(W_w - W_d)/d_w}{(W_w - W_d)/d_w + W_d/d_p} \times 100\% \tag{4}$$

Table 1
The composition of the solutions used for the membrane preparations

Type of membrane	Applicator gap width (mm)	Amount of GO in PAN/DMF solution (g)	Amount of PAN (g)	Concentration of GO (% w/w)	Concentration of PAN (% w/w)
"0"	0.2	0.0	12.0	0.0	100.0
	0.3				
A	0.2	0.1	12.0	0.8	99.2
	0.3				
B	0.2	0.5	12.0	4.0	96.0
	0.3				
C	0.2	1.0	12.0	7.7	92.3
	0.3				

where d_w is the density of distilled water (0.998 g/cm^3) and d_p is the polymer density (1.184 g/cm^3) [9].

2.5. Measurements of water flux

The transport properties of the formed membranes were tested using a Millipore Amicon 8400 UF cell with a 350 mL capacity and a 7.6 cm membrane diameter that was equipped with an equalizing tank with an 800 mL capacity. First, dry membranes were immersed in distilled water for 1 h. Then, they were treated with distilled water for an additional 2 h under a pressure of 0.2 MPa to improve the membrane stability. UF tests were performed at operational pressures of 0.1, 0.15, or 0.2 MPa. Permeate flux (J_v) was calculated using the following equation:

$$J_v = \frac{Q}{A \times t} \tag{5}$$

where J_v is water flux (L/m^2 × h), Q is the permeate volume (L), A is the effective membrane area (m^2), and t is the permeation time (h).

Pore size (r_m) was calculated on the basis of the specific permeate flux and porosity using the Guerout–Elford–Ferry equation [52]:

$$r_m = \sqrt{\frac{(2.9 - 1.75\varepsilon) \times 8\eta l Q}{\varepsilon \times A \times \Delta P}} \tag{6}$$

here η is the water viscosity (8.9 × 10^{-4} Pa·s), l is the membrane thickness (m), Q is the volume of permeated pure water per unit time (m^3/s), A is the effective membrane area (m^2) and ΔP is the operational pressure.

2.6. Measurements of rejection

Studies of membrane transport properties using anhydrous FeCl$_3$ aqueous solution with a concentration of 0.1 g/L were also conducted. The FeCl$_3$ solution was poured into the UF cell with a previously tested membrane. The contents of the UF cell were mixed using a magnetic stirrer to prevent fouling. The permeation process was conducted by successively removing 5 mL batches of permeate, simultaneously measuring the time of the permeate flow from the testing tank. The permeate flux (J_v) was calculated using Eq. (5), assuming that in this case, Q is the permeate volume (FeCl$_3$ solution) per unit time (m^3/s) and ΔP is the operational pressure (0.2 MPa).

The concentration of FeCl$_3$ in the permeate was determined using UV–Vis spectrophotometry by measuring the absorbance at 280 nm. Based on the calibration curve, the concentrations of ferric ions in each sample were calculated. Then, using Eq. (7), the rejection performance (R) for FeCl$_3$ was calculated, which is closely associated with the occurrence of fouling.

$$R = \left(1 - \frac{C_p}{C_f}\right) \times 100\% \tag{7}$$

where R is the rejection performance of the membrane (%) and C_p and C_f are the concentrations of FeCl$_3$ in the permeate and feed solution (g/L), respectively.

2.7. Analytical methods

All measurements were performed using a Nicolet 6700 FT-IR spectrometer (Thermo Electron Corp., Madison, WI, USA) with an attenuated total reflectance (ATR) accessory equipped with a multiple bounce crystal of KRS (TlBrI) and an angle of incidence of 45°. The following measurement parameters were used: resolution, 4 cm^{-1}; spectral range, 500–4,000 cm^{-1}; (DTGS) detector; number of scans, 256. Data collection and post-processing were performed using OMNIC software (v. 8.0, Thermo Electron Corp.).

Raman spectroscopy was performed with a Renishaw InVia micro-Raman spectrometer, with an excitation laser at 633 nm, a laser power of approximately 15 mW, a spectral resolution of 2 cm^{-1}, and a long working distance objective Olympus LMPLFLN 20X.

X-ray diffraction (XRD) investigations were performed with a URD 63 Seifert diffractometer. Cu Kα radiation was used at 40 kV and 30 mA. Monochromatization of the beam was obtained by means of a nickel filter and a pulse-height analyzer. A scintillation counter was used as a detector. Diffractograms were recorded from 18° to 26° with a step of 0.01°. Each diffraction curve was corrected for polarization, the Lorentz factor, and incoherent scattering.

Thermal studies of the membranes were conducted using a TA Instruments MDSC 2920 differential scanning calorimeter (DSC). The DSC curves obtained were analyzed using the TA Instruments Universal v4.5 software package. Measurements were performed under a nitrogen atmosphere (flow rate 40 mL/min) while heating at 10°C/min from −10°C to 320°C.

Membrane surface morphologies and their cross-sections were observed using a JSM 5500 LV JEOL scanning electron microscope. All samples were coated with a layer of gold in a JEOL JFC 1200 vacuum coater at 3 × 10^{-5} Torr.

The concentration of FeCl$_3$ in the permeate was determined using a Perkin Elmer Lambda 35 UV–Vis spectrophotometer.

3. Results and discussion

3.1. Characteristics of GO

GO, which was used to prepare GO/PAN composite membranes, was studied using XRD, DSC thermal analysis, and FTIR spectroscopy. The analysis results were very similar to the ones obtained in our earlier work [49].

3.2. Membrane characteristics

This paper describes extensive characteristics of GO/PAN composite membranes produced through the phase inversion coagulation of a polymer solution. Membranes were prepared from a PAN solution in DMF containing dispersed GO nanoparticles. Our study shows how the concentration of GO affects the structure and physicochemical properties of the obtained membranes. The following measurements and calculations were recorded: thickness, mass per unit area, density, sorption, porosity, pore size, and specific permeate flux measured in the distilled water and an aqueous solution of FeCl$_3$.

We determined that even a small addition of GO affects the membrane coagulation process, resulting in an increase

in the mass per unit area (Fig. 2(a)). For membrane A, containing 0.8% w/w GO in a solution of PAN/DMF, there is a slight increase in the mass of the formed membrane regardless of the thickness of the polymer film. Increasing the amount of GO to 4% w/w results in an approximately 50% increase in the mass per unit area for membrane B prepared with an applicator gap width of 0.2 mm (B-0.2). In contrast, membrane B prepared with a larger applicator gap width, that is, 0.3 mm (B-0.3 membrane), is characterized by a 10% increase in the mass per unit area compared with the pure PAN membrane ("0"-0.3 membrane). Increasing the concentration of GO to 1:12 parts w/w in the PAN/DMF solution did not significantly affect the mass per unit area when the membrane was formed into a 0.2 mm film. However, in the case of the C-0.3 membrane processed from the 0.3 mm film, an 80% increase in mass per unit area was observed with respect to

the reference membrane ("0"-0.3). The study shows that for the applicator gap width of 0.2 mm, the greatest masses per unit area were characteristic for membranes B-0.2 and C-0.2. However, the membrane formed using the 0.3 mm gap width applicator and containing 7.7% of GO (C-0.3) had the highest mass of all the examined membranes.

Comparing our results with the results of work from Feng et al. [65], it can be concluded that more hydrophobic polymers coagulate more rapidly. The studies show that the lowest of the GO additions used has little effect on the membrane coagulation, as the membranes A are similar in terms of mass per unit area. The difference in mass per unit area starts to occur at the 1:24 and 1:12 ratios of GO. GO present in the polymer matrix is responsible for the strong hydrophilization of the polymer solution, which is most visible for the C-0.3 membrane.

Analyzing the thickness measurements of all studied membranes (Fig. 2(b)), the GO addition has a strong impact on this parameter. Even a small addition of GO into the polymer matrix causes more than a 4.5-fold increase in the thickness of membrane A-0.2 and more than a 3-fold increase in the thickness of membrane A-0.3. Larger contents of GO cause further increases in the thickness of the resulting membranes. For membranes formed using the applicator with a 0.2 mm gap width, the increase in thickness is 550% for membrane B and 600% for membrane C. The increases in thickness of membranes formed from a thicker polymer film (0.3 mm) are 350% and 430% for the B-0.3 and C-0.3 membranes, respectively. The large increase in thickness of membranes upon GO addition for all membranes formed using the 0.2 mm gap width applicator is due to the facilitated penetration of the coagulant into the thinner film and changes in the hydrophilic properties of the membrane. GO is strongly hydrophilic, resulting in the membrane coagulation process slowing down. The observed phenomenon was described by Feng et al. [65] in a study on polyphenylsulfone (PPSU) membranes. However, for membranes formed using the 0.3 mm gap width applicator, their thickness also increases, but because of the thick layer of the processed films, the observed values are slightly lower.

The mass and thickness measurements allowed the density of the examined membranes to be calculated (Fig. 2(c)). When comparing the results, it is evident that membranes made from pure PAN have the highest densities, which means they are the most compact. The densities of the other membranes are reduced by approximately two-thirds and have very similar values. The low densities and high thicknesses of all the GO/PAN membranes may indicate high porosity in these membranes.

Fig. 3 demonstrates that the porosity of pure polyacrylonitrile membranes is 85% (membrane "0"-0.2) and 83% (membrane "0"-0.3). Comparing the thickness, density and porosity of the "0" membranes, it may be assumed that the membranes contain many small pores. Analysing the other membranes, it can be observed that the addition of GO causes a slight decline in the porosity value from approximately 83%, through 81%, to 80.5% for the following membranes: A-0.2, B-0.2, C-0.2. For the thicker membranes, however, the decrease is higher and proceeds from 82% (A-0.3), to approximately 78.5% (B-0.3) through to 77% (C-0.3). Notably, looking at all the results, all the membranes with GO addition are
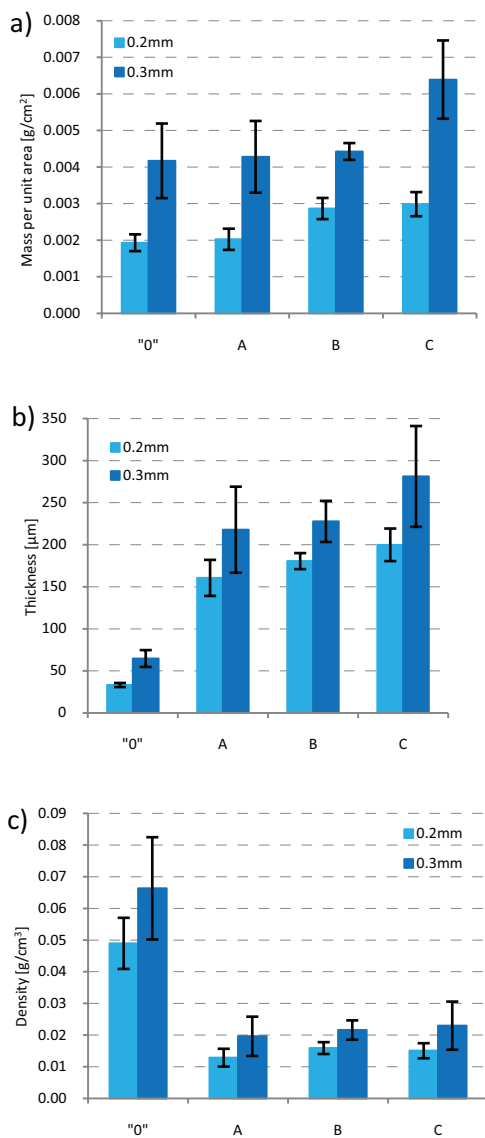
Fig. 2. Effect of GO addition on: (a) the mass per unit area, (b) the thickness, and (c) the density of membranes.

characterized by high porosity from 77% to 85%. Comparing the thickness and density values with the porosity of the composite GO/PAN membranes, it can be assumed that they are all composed of large pores, whose size will increase with the amount of GO addition.

In examining the sorption properties of all the obtained membranes (Fig. 3(b)), it must be emphasized that the values are very high, 300%–500%. The membranes prepared from pure polyacrylonitrile display the best sorption properties: 493.14% ± 51.64% and 438.19% ± 42.22% for the "0"-0.2 and "0"-0.3 membranes, respectively. Comparing the polyacrylonitrile sorption values with those used in our earlier study [64], it can be seen that the type of PAN copolymer has a very strong influence on the properties of the membrane. In both cases, the same polymer concentrations and the same solvent were used, and for membranes obtained from a copolymer containing 93%–94% acrylonitrile/5%–6% methyl acrylate/1% sodium allyl sulfonate, M_w = 50,000, and water sorption was 352.69% ± 5.16% for a 0.2 mm applicator gap width. Analysing the water sorption values of the composite GO/PAN membranes, it can be seen that with increasing GO concentration in the polymer matrix, the sorption properties decline. The highest sorption is characteristic of membranes A, 428.21% ± 46.77% for membrane A-0.2 and 397.79% ± 31.84% for membrane A-0.3, which also have the lowest density and the highest porosity. Membranes C, on the other hand, which have the highest density of all membranes with GO addition, are characterized by the lowest water sorption. Moreover, membranes C display the lowest porosity. All the results from studying the physicochemical properties of the C-0.2 and C-0.3 membranes indicate that their water

sorptions had the lowest values: ~360% for the thinner membrane and ~290% for the thicker one.

3.3. Transport properties and pore sizes of membranes

An important parameter determining the transport properties of membranes is the specific permeate flux (Fig. 4(a)). Membranes A, which contained the lowest nano GO addition, exhibited specific permeate flux values of 1.65, 1.94 and 2.28 L/m² × h for membrane A-0.2 at operational pressures of 0.10, 0.15, and 0.20 MPa, respectively. Compared with the results for the membranes made from pure PAN ("0"-0.2), we can observe 3.5-, 4.5-, and 5-fold decreases in the specific permeate flux values. The results may be due to interactions between PAN and GO that impede transport through the membrane. Further increases in the GO concentration in composite GO/PAN membranes cause increases in the specific permeate flux. The highest permeate flux values are the ones for membrane C. For membrane C-0.2, they are equal to 5.92 ± 0.12; 8.30 ± 0.08, and 10.52 ± 0.17 L/m² × h for operational pressures of 0.10, 0.15, and 0.20 MPa, respectively. For these membranes, the permeate flux values compared with pure PAN membrane are increased by 40%, 12%, and 9%, respectively, for the various working pressures of the membrane. The obtained results may indicate that with the increase in the pressure at which the membrane is operated, it is being crushed, which impedes the water flow. For membranes formed using the 0.3 mm gap width applicator, an increase in the specific permeate flux values can be observed with increasing GO concentration. The permeate flux values for the A-0.3 membranes are very similar to those obtained for "0" membranes. Comparing the transport properties with
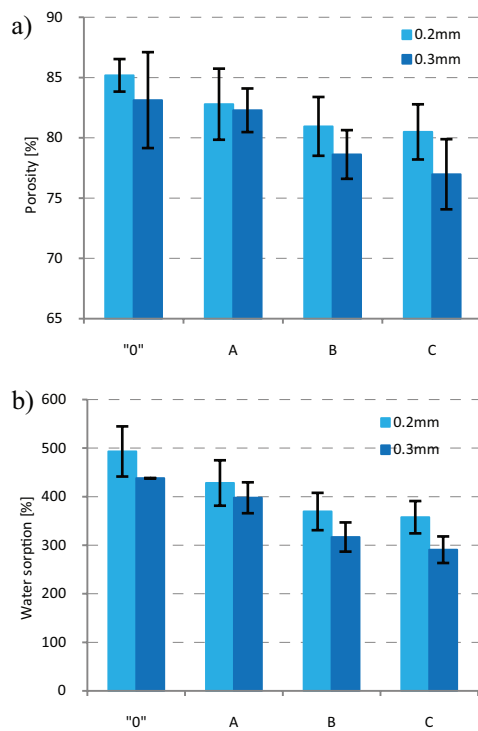

Fig. 3. Effect of GO addition on (a) the porosity of the membranes and (b) the sorption of water.
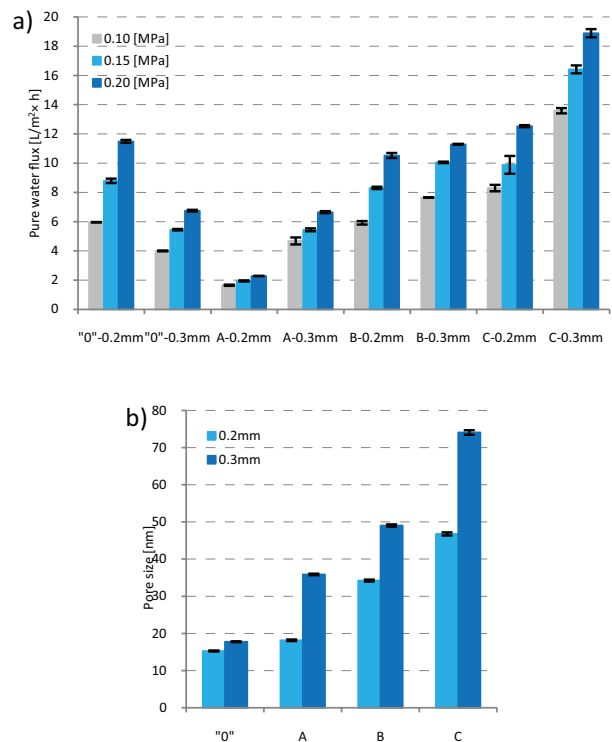

Fig. 4. Test results of (a) water flux and (b) membrane pore sizes.

the porosity and water sorption values, it is evident that all the parameters of the membranes ("0"-0.3 and A-0.3) mentioned above have similar values. The specific permeate fluxes for membrane B-0.2 are 7.65 ± 0.01, 9.65 ± 0.05, and 12.29 ± 0.01 L/m² × h for the given pressures (0.10, 0.15, and 0.20 MPa), that is, increases by 90%, 77%, and 68% relative to membrane "0"-0.3. Furthermore, for C-0.3 membranes, additional 240%, 200%, and 180% increases in the determined flux at operational pressures of 0.10, 0.15 and 0.20 MPa are observed. Thus, in each case, the membranes may be crushed under operational water pressure.

The transport property studies lead to the conclusion that additional GO has no effect on the specific permeate flux if the membranes are formed using an applicator with a 0.2 mm gap width. For membranes molded using an applicator with a 0.3 mm gap, however, there is a steady increase in the transport properties with increasing nano GO concentration in the GO/PAN membrane. The specific permeate flux can also be explained in another way. During the formation of membranes using phase inversion – the wet method – the coagulation process speed is known to depend on the thickness of the polymer film. Therefore, in this case, all the composite GO/PAN membranes formed using the 0.3 mm gap width applicator coagulate slower than those formed with the 0.2 applicator. The longer coagulation may provide the additional time necessary an arrangement of GO nanoparticles that can better facilitate the transport of liquid through the membrane.

Pore size is a parameter that impacts variables such as porosity, thickness, or specific permeate flux; for the studied membranes, the estimated pore sizes are presented in Fig. 4(b). The pristine polyacrylonitrile "0"-0.2 membrane has the smallest pore size, 15.3 nm, and the "0"-0.3 membrane has a pore size of 17.8 nm (Fig. 4). Comparing these results with those described by Fryczkowska et al. [64], it appears that the pore sizes are doubled, confirming that the type of polymer used has a decisive influence on all parameters of the obtained membrane. The pore sizes of the composite GO/PAN membrane molded using the 0.2 mm gap width applicator increase with the increase in added GO and equal 18.1–46.8 nm, whereas for thicker membranes (0.3 mm), they are in the range of 35.3–74.1 nm. The calculations allowed us to conclude that the addition of GO evidently affects the morphology of the membrane structure. Of the thin membranes, the pore size of the A-0.2 membrane is comparable with that of the pure "0"-0.2. membrane. If we examine the results, the GO scarcely affects the pore size; it slightly reduces the water sorption as well as the calculated porosity of the A-0.2 membrane and reduces the specific permeate flux by 5–3.5 times, depending on the applied pressure. This is probably related to the thin surface layer of membrane A-0.2. However, with a larger quantity of GO addition, the pore size increases by approximately 124% for membrane B-0.2 and 306% for membrane C-0.2. Such a pore size may explain the transport properties of membranes with GO, which gradually improve with the addition amount. Perhaps, after exceeding a certain amount of GO, a thin layer of GO on the surface of the membrane surface layer alters the characteristics by increasing the concentration of the oxide, which slowly begins to agglomerate. As a result of this process, "channels" are formed through which water transport is facilitated.

For thicker membranes (0.3 mm), the calculated pore size increases by 102%, 175%, and 336%. This increase in the pore size is correlated with an increase in the density of the membranes, and therefore, in these conditions, large pores may be formed with thick walls to prevent being crushed during the permeation process. Such a membrane structure is also confirmed by the water sorption and porosity, which decrease with an increasing concentration of GO in the membrane.

3.4. Rejection of Fe^{3+} ion

In the Fe^{3+} rejection experiments, the transport property testing was performed by using an aqueous solution of iron salt ($FeCl_3$) at a concentration of 0.1 g/L. During the tests, the specific permeate flux was determined (Fig. 5) in addition to the retention performance (Fig. 6).

Studies have shown that introducing a solution of iron ions to pure PAN and GO/PAN membranes resulted in increases in the specific permeate flux (Fig. 5). The transport properties at the beginning of the measurements increased in comparison with the results for distilled water. Observing the specific permeate flux values while passing a solution of iron ions through the "0"-0.2 membrane, we can see that the flow decreases with time to approximately 11.6 L/m² × h, a value very similar to the flow of distilled water. Tor the thicker membranes ("0"-0.3), the membrane
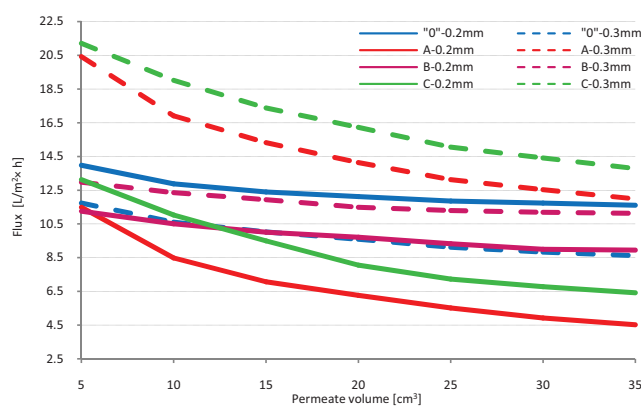

Fig. 5. Volumetric permeate flux of $FeCl_3$ solution (at an operational pressure of 0.2 MPa).
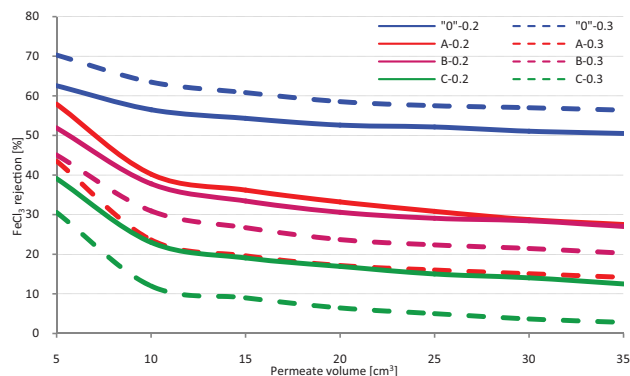

Fig. 6. Degree of $FeCl_3$ rejection.

operation stabilization during the transport of the ferric ions occurs at higher specific permeate flux values, namely, 8.6 L/m² × h. Such results may confirm that the pore sizes determine the transport properties. Analysing the results of the studies, the curves for membranes B-0.2 and B-0.3 appear similar in shape to the curves representing membranes "0"-0.2 and "0"-0.3. The permeate flux values also decrease when a solution of ferric ions is passed through, with membrane B-0.3 demonstrating a value of 11.1 L/² × h, which is similar to the flow calculated for the distilled water. However, for a thinner membrane (B-0.2), the specific permeate flux falls slightly below the values for pure water, which is approximately 9.0 L/m² × h. This behavior of the GO/PAN composite membranes may indicate the adsorption of ferric ions within the small pores of membrane B-0.2. The highest increase in the specific permeate flux (5-fold increase) was observed for membrane A-0.2, whereas for membrane A-0.3, a 3-fold increase was recorded. These results clearly indicate a change in the nature and charge of such membranes that favors the transport of iron ions. During operation, there are decreases in the transport properties to 4.5 and 12 L/m² × h, respectively, for membranes A-0.2 and A-0.3. These values are approximately 2 times higher compared with the specific permeate flux of clean water. Thus, one can surmise that during the permeation, ferric ion adsorption can occur on the membranes, which does not interfere with the permeate flow. The specific permeate flux results for membranes A and C, illustrated in Fig. 5, show that curves of J_v related to permeate volume relation are similar. However, for membrane C, the permeate flux is reduced during operation of the membranes. For membrane C-0.2, it is reduced almost twice, to approximately 6.4 L/m² × h, whereas for thicker membranes (C-0.3), the reduction is lower, to approximately 13.8 L/m² × h. The obtained values of specific permeate flux may be related to pore size, which is higher for thicker membranes.

The rejection (*R*) for iron(III) ions on the membranes can be seen in Fig. 6. The highest rejection values reach 70.30%–56.38% and 62.56%–50.48% for membranes "0"-0.3 and "0"-0.2, respectively. However, the rejection by the GO/PAN composite membranes drops sharply, by 30%–60%, at the beginning of the membrane operation and then slowly stabilizes. The highest retention rate values were obtained for membranes containing the highest GO addition (membrane C). The obtained results correspond to those of Zhao et al. [66]. Such behavior of the GO/PAN composite membranes indicates that GO undoubtedly affects the performance of the membrane, facilitating the transport of ferric ions. Thus, for the studied membranes, the fouling process does not occur. The behavior of the membranes under the influence of an aqueous solution of FeCl₃ can be explained by coordinating interactions between oxygen functional groups of GO and permeating ions of various metals, as described in the literature. Mo et al. [48] studied the effect of electrolytes containing sodium, potassium, magnesium, and calcium ions on the membrane operation and arrangement of GO layers to explain the observed membrane transport phenomenon. Similar studies were also presented by Mahmoud et al. [37]. One can therefore presume that coordination bonds may be formed between the electronegative PAN membrane and GO.

Pictures of membranes after UF of FeCl₃ solutions are shown in Fig. 7. The image of the pure PAN ("0") membrane reveals an orange coloration arising from Fe^{3+} ions, which precipitate on the membrane to form the fouling as described earlier (Fig. 6). However, in the case of GO/PAN composite membranes, the deposition of iron ions on the membrane decreases with the concentration of GO in the membrane. These observations confirm the results of our studies, clearly indicating the anti-fouling properties of GO/PAN membranes.

3.5. SEM analysis

The use of scanning electron microscopy (SEM) allowed us to examine the surface and cross-section morphology of the studied composite GO/PAN membranes. SEM images (Fig. 8) confirm the asymmetric construction of all membranes. For membrane "0", a dense skin layer with a thickness of 2.5–3.0 μm is clearly visible, whereas in the images and cross-sections of composite membranes, in the skin layer, a surface coated with a vast amount of very small capillaries is observed. Images of the skin side of membranes show a smooth, flat surface for membrane "0", while for the composite GO/PAN membranes, uneven and hollow areas without any visible pores on the skin layer are observed. The structure and morphology of the support layer is even more interesting. The surface of the support layer of membrane "0" is heavily creased, and at higher magnifications, distinct pores are visible, whereas the surfaces of the composite membranes consist of easily visible, sizable pores, and at higher magnifications, a very interesting, multidimensional structure can be seen.
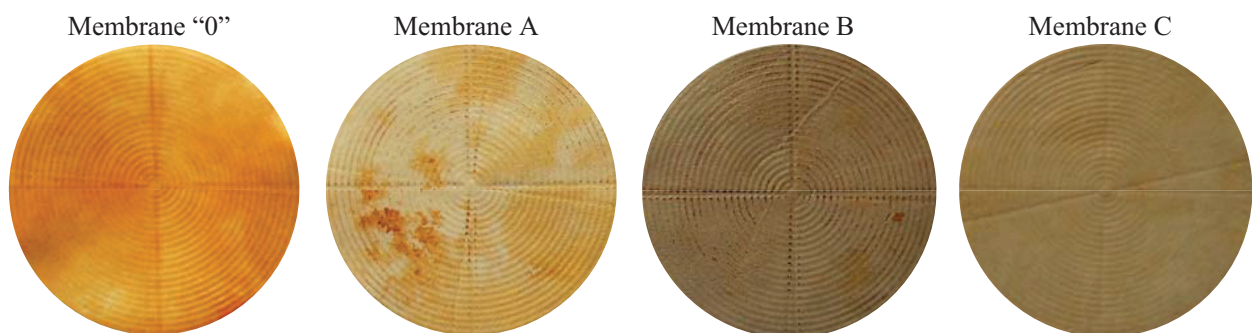
| Membrane "0" | Membrane A | Membrane B | Membrane C |

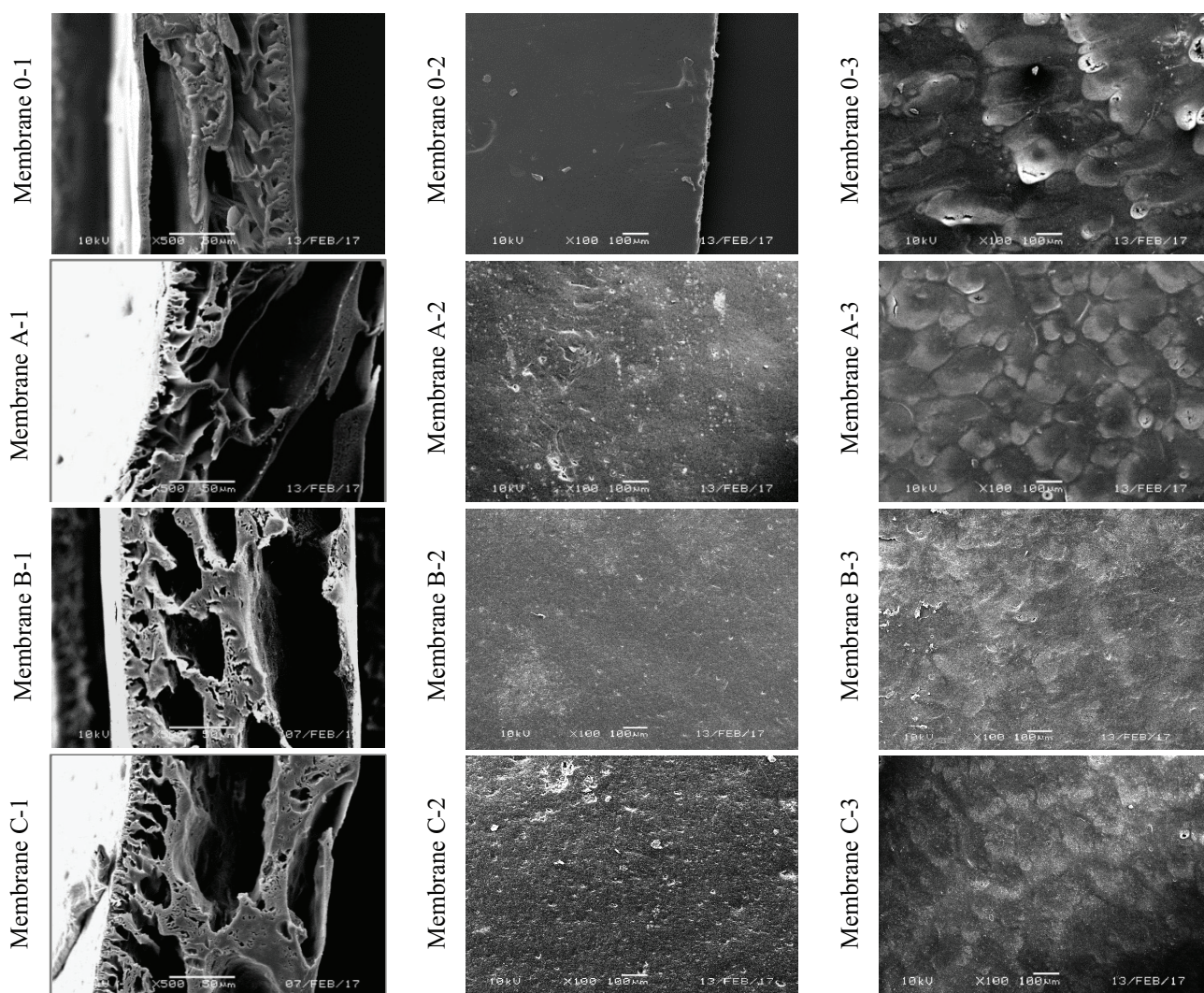Fig. 7. The surface of membranes after UF experiments of FeCl₃ solution.

Fig. 8. Images (SEM) of pure PAN and GO/PAN composite membranes: (1) cross-section; (2) top (skin) layer; (3) bottom layer.

3.6. ATR–FTIR analysis

The molecular structure of the skin surface was determined using an attenuated total reflectance Fourier transform infrared spectroscopy (ATR–FTIR) method. In the spectra (Fig. 9), characteristic absorption bands can be observed via the oscillators in PAN. The band at 2,925 cm^{-1} corresponds to C–H oscillator stretching vibrations, 2,243 cm^{-1} reflects C≡N oscillator stretching vibrations, and 1,450 cm^{-1} and 1,360 cm^{-1} are the deformation vibrations of CH$_2$ and CH groups [30,56], respectively. In the GO spectrum, a wide band at approximately 2,800–3,400 cm^{-1} reflects oscillations of the OH group. In the analysis of the spectral bands of PAN and its blends with GO, the introduction of GO into the PAN matrix clearly reduces the intensity of the C≡N oscillator band. The intensity of the discussed bands decreases, starting from the spectrum of membrane A and continuing through the spectra of membranes B and C. This observed phenomenon may be due to the formation of unstable coordination bonds between the polymer matrix and GO functional groups. In the spectra of composite membranes, a broad but weak band at 1,376 cm^{-1} is present,

associated with the epoxy or ether groups existing in the chemical structure of GO [39]. Another frequency characteristic for the C=O oscillator of the carbonyl groups in GO is the signal at 1,650 cm^{-1}, whose intensity increases with the addition of GO in subsequent membranes. The band at approximately 1,730 cm^{-1} appearing in the spectra is the characteristic of stretching vibrations of the C=O oscillator in ester groups [30] and can be derived from raw PAN (copolymer containing approximately 6% of the ester) and GO [39]; hence, the difference in the intensity compared with the other bands. The appearance and intensity of this band indicate the presence of GO on the surface of composite GO/PAN membranes to a depth comparable with the wavelength of the measurement beam.

3.7. Raman spectroscopy analysis

Raman spectroscopy (Fig. 10) revealed characteristic GO bands: ~1,340 cm^{-1} (D line) and ~1,594 cm^{-1} (G line) [67]. In the Raman spectrum of the pure PAN (membrane "0"), characteristic peaks appear: ~1,665, ~1,450, ~1,360, and, 1,320 cm^{-1} [58].

The spectra of the GO/PAN composite membranes contain characteristic peaks for both components of the composite. The G peak is single and sharp and occurs at approximately 1,580–1,594 cm^{-1}. In contrast, the D peak is wide and flat for membranes A and B, which contain 0.8% and 4% GO w/w. For membrane C, a single and strong peak from GO is observed. In addition, the spectra for all GO/PAN composite membranes include a ~1,450 cm^{-1} peak, which comes from the PAN. Ionita et al. [68] also observed the occurrence of a double peak in Raman spectra of composites containing GO.

The integral area of D band and G band (ID/IG) peak intensity height ratio for GO is 0.97, while the D:G peak area ratio is 1.81. For the GO/PAN composite membranes, the ID/IG intensity height ratio increases as the GO concentration increases in the polymer matrix, from 1.06 (membrane A) to 1.10 (membrane B) and then 1.11 (membrane C). Comparing the peak areas ratio, the results were, respectively, 2.04, 2.11, and 2.20 for membranes A, B, and C. Our studies show that the polymer matrix interacts with GO, increasing the number of defects in its structure.

3.8. WAXS analysis

Fig. 11 shows wide-angle X-ray scattering (WAXS) diffraction curves of membrane "0" (pristine PAN), GO and the composite GO/PAN membrane C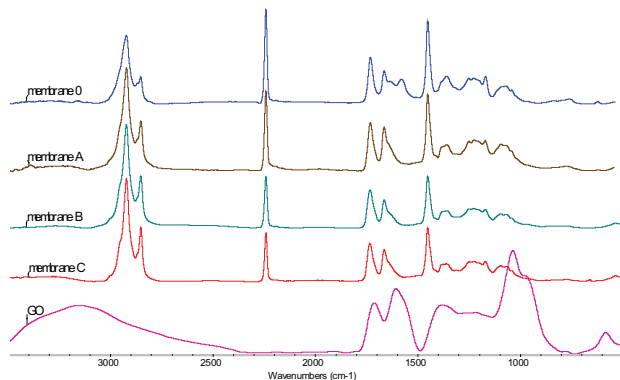 with the highest GO content. In the diffraction curve of membrane "0", a sharp, intense peak at 16.7° and a weak peak at 28.5° can be seen. The first peak corresponds to the (100) diffraction of the hexagonal lattice, and the second peak is ascribed to the second-order diffraction of the first peak [69]. The XRD pattern of the composite membrane shows an additional peak at 10.5°, corresponding to the (002) reflection of GO while still presenting the PAN peaks at 16.7° and 28.5°. The appearance of both PAN and GO peaks indicates that the structure of GO and the PAN chains did not change during the membrane formation.

3.9. DSC analysis

Fig. 12 summarizes the DSC curves recorded during the calorimetric tests. For all tested membranes, at temperatures just below 300°C, the curves show a very strong exothermic peak, which is the dominant element of the thermogram. The discussed thermal effect reflects the PAN cyclization reaction that occurs during heating. Lee et al. [31] studied the influence of GO on the PAN cyclization reaction. According to these researchers, the PAN homopolymer cyclized as a result of free-radical reaction at 306.2°C. In our case, the commercial PAN used to prepare membranes is a copolymer of acrylonitrile with methyl acrylate and methallyl sulfonate, and its cyclization occurs at 294.2°C with a specific enthalpy of cyclization of 576.1 J/g. However, the temperature of cyclization of the composite membranes is slightly lower, at 293.8°C, 293.4°C, and 289.1°C for membranes A, B, and C, respectively. The observed changes in cyclization temperature in the presence of GO are in agreement with the results for composite membranes described by Lee et al. [31]. In our previous studies, we demonstrated that at a temperature of approximately 185°C, there is a partial reduction of pure GO [70]. In the present study, DSC curves recorded for composite membranes B and C (Fig. 12), an additional, relatively weak exothermic peak with a maximum at 216.9°C or 180.7°, respectively, can also be observed. These peaks probably correspond to the reduction of GO in composite membranes. The shift in the position of the maxima from these effects can be explained by the different compositions of the examined membranes and GO [31]. The determined specific enthalpy of GO reduction for membrane B is 58.3 J/g, while for membrane C, it is 58.8 J/g.

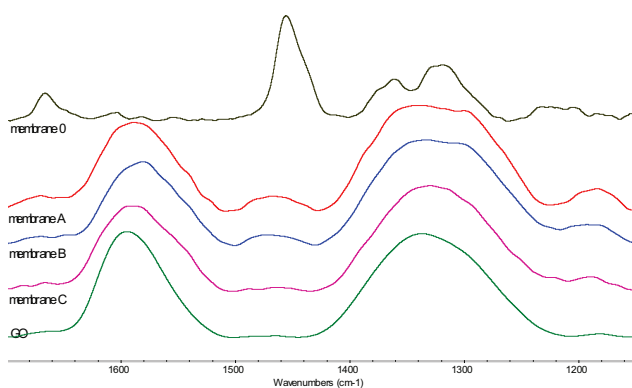Fig. 9. ATR–FTIR spectra of the GO, composite GO/PAN membranes and pristine PAN membrane.

Fig. 10. The Raman spectra of the GO, the GO/PAN A, B and C composite membranes and the pristine PAN membrane.

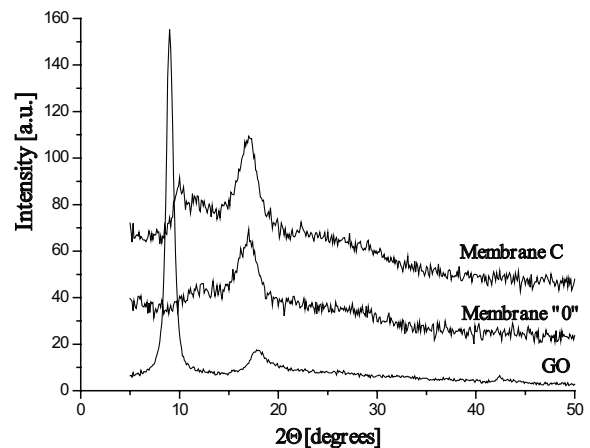

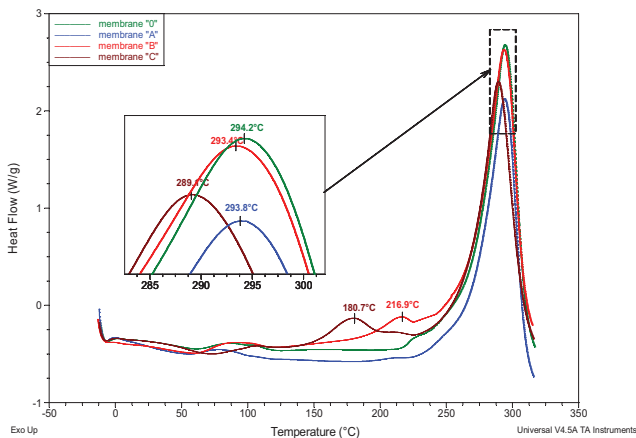Fig. 11. WAXS patterns of PAN, GO and GO/PAN composite membranes.

Fig. 12. DSC curves of the GO/PAN composite and pristine PAN membranes.

4. Conclusion

This paper presents results of research on the effect of the presence of GO on the properties of composite PAN membranes. The membranes were prepared by a phase inversion method from a dispersion of GO in PAN solution in DMF, using distilled water as a coagulation bath. The advantages of this technique are its simplicity and the durability of the links between the composite components. The investigated membranes varied in composition, structure, and physicochemical and transport properties. Effect of GO addition on the coagulation process was observed, resulting in increases in mass per unit area and thickness and decreases in density, sorption properties and porosity of the composite GO/PAN membranes. The noticeable differences in morphology and structure in the SEM images confirmed the observed changes in the composite membranes' physicochemical properties. A significant increase in the specific permeate flux, equal to 12.53–18.89 L/m^2 × s, and the largest pore sizes (46.8–74.1 nm) were characteristic for membrane C, which contained the highest amount of GO. The qualitative studies of the composition of the membranes using an ATR–IR technique proved the occurrence of GO on the surface of GO/PAN membranes. DSC studies confirmed that GO incorporated into the PAN matrix at a level of at least 4% influences the properties of the polymer, lowering the temperature of the PAN cyclization reaction.

An interesting phenomenon was observed for the permeation of FeCl$_3$ solution through the GO/PAN composite membranes. At the beginning of UF, the specific permeate flux was high, and it then quickly fell and stabilized. At the same time, the retention of Fe^{3+} ions was low, indicating that GO/PAN membranes are unlikely to cause fouling. Thus, the unusual behavior of the composite membranes is caused by the addition of GO. Our studies allow us to propose that the formation of unstable coordination bonds between the PAN matrix and the GO functional groups is possible and results in the changed nature of the resulting composite membrane. The formation of coordination interactions between GO in the composite GO/PAN membrane and Fe^{3+} ions is also possible, which prevents the occurrence of fouling.

References

[1] V. Bhanu, P. Rangarajan, K. Wiles, M. Bortner, M. Sankarpandian, D. Godshall, T. Glass, A. Banthia, J. Yang, G. Wilkes, Synthesis and characterization of acrylonitrile methyl acrylate statistical copolymers as melt processable carbon fiber precursors, Polymer (Guildf), 43 (2002) 4841–4850.
[2] P. Gibson, H. Schreuder-Gibson, D. Rivin, Transport properties of porous membranes based on electrospun nanofibers, Colloids Surf., A, 187–188 (2001) 469–481.
[3] S.K. Nataraj, K.S. Yang, T.M. Aminabhavi, Polyacrylonitrile-based nanofibers—a state-of-the-art review, Prog. Polym. Sci., 37 (2012) 487–513.
[4] J.-J. Hwang, T.-W. Ma, Preparation, morphology, and antibacterial properties of polyacrylonitrile/montmorillonite/silver nanocomposites, Mater. Chem. Phys., 136 (2012) 613–623.
[5] L. Feng, S. Li, H. Li, J. Zhai, Y. Song, L. Jiang, D. Zhu, Super-hydrophobic surface of aligned polyacrylonitrile nanofibers, Ang. Chem. Int. Ed. 41 (2002) 1221–1223.
[6] Y. Yang, H. Wang, X. Lu, Y. Zhao, X. Li, C. Wang, Electrospinning of carbon/CdS coaxial nanofibers with photoluminescence and conductive properties, Mater. Sci. Eng., B, 140 (2007) 48–52.
[7] J.S. Im, S.-J. Park, T.J. Kim, Y.H. Kim, Y.-S. Lee, The study of controlling pore size on electrospun carbon nanofibers for hydrogen adsorption., J. Colloid Interface Sci., 318 (2008) 42–49.
[8] S. Lee, J. Kim, B.-C. Ku, J. Kim, H.-I. Joh, Structural evolution of polyacrylonitrile fibers in stabilization and carbonization, Adv. Chem. Eng. Sci., 2 (2012) 275–282.
[9] G. Wypych, Handbook of Polymers, ChemTec Publishing, Ontario, Canada, 2012, pp. 271–275.
[10] M.M. Iovleva, V.N. Smirnova, G.A. Budnitskii, The solubility of polyacrylonitrile, Fibre Chem., 33 (2001) 262–264.
[11] Y. Eom, B.C. Kim, Solubility parameter-based analysis of polyacrylonitrile solutions in N,N-dimethyl formamide and dimethyl sulfoxide, Polymer, 55 (2014) 2570–2577.
[12] T.D. Tran, S. Mori, M. Suzuki, Plasma modification of polyacrylonitrile ultrafiltration membrane, Thin Solid Films, 515 (2007) 4148–4152.
[13] K. Nouzaki, M. Nagata, J. Arai, Y. Idemoto, N. Koura, H. Yanagishita, H. Negishi, D. Kitamoto, T. Ikegami, K. Haraya, Preparation of polyacrylonitrile ultrafiltration membranes for wastewater treatment, Desalination, 144 (2002) 53–59.
[14] I.-C. Kim, H.-G. Yun, K.-H. Lee, Preparation of asymmetric polyacrylonitrile membrane with small pore size by phase inversion and post-treatment process, J. Membr. Sci., 199 (2002) 75–84.
[15] H.-A. Tsai, Y.-L. Ye, K.-R. Lee, S.-H. Huang, M.-C. Suen, J.-Y. Lai, Characterization and pervaporation dehydration of heat-treatment PAN hollow fiber membranes, J. Membr. Sci., 368 (2011) 254–263.
[16] H. Lohokare, Y. Bhole, S. Taralkar, U. Kharul, Poly(acrylonitrile) based ultrafiltration membranes: optimization of preparation parameters, Desalination., 282 (2011) 46–53.
[17] P. Wang, Z. Wang, Z. Wu, Insights into the effect of preparation variables on morphology and performance of polyacrylonitrile membranes using Plackett–Burman design experiments, Chem. Eng. J., 193–194 (2012) 50–58.
[18] S. Yang, Z. Liu, Preparation and characterization of polyacrylonitrile ultrafiltration membranes, J. Membr. Sci., 222 (2003) 87–98.
[19] D. Pal, S. Neogi, S. De, Surface modification of polyacrylonitrile co-polymer membranes using pulsed direct current nitrogen plasma, Thin Solid Films, 597 (2015) 171–182.
[20] W.-S. Hung, Q.-F. An, M. De Guzman, H.-Y. Lin, S.-H. Huang, W.-R. Liu, C.-C. Hu, K.-R. Lee, J.-Y. Lai, Pressure-assisted self-assembly technique for fabricating composite membranes consisting of highly ordered selective laminate layers of amphiphilic graphene oxide, Carbon, 68 (2014) 670–677.

[21] M. Hu, B. Mi, Layer-by-layer assembly of graphene oxide membranes via electrostatic interaction, J. Membr. Sci., 469 (2014) 80–87.

[22] C.-L. Lai, W.-C. Chao, W.-S. Hung, Q. An, M. De Guzman, C.-C. Hu, K.-R. Lee, Physicochemical effects of hydrolyzed asymmetric polyacrylonitrile membrane microstructure on dehydrating butanol, J. Membr. Sci., 490 (2015) 275–281.

[23] F. Zhang, S. Gao, Y. Zhu, J. Jin, Alkaline-induced superhydrophilic/ underwater superoleophobic polyacrylonitrile membranes with ultralow oil-adhesion for high-efficient oil/water separation, J. Membr. Sci., 513 (2016) 67–73.

[24] O.C. Compton, S.T. Nguyen, Graphene oxide, highly reduced graphene oxide, and graphene: Versatile building blocks for carbon-based materials, Small, 6 (2010) 711–723.

[25] W. Gao, The Chemistry of Graphene Oxide, Graphene Oxide Reduction Recipes, Spectroscopy Applications, Springer International Publishing, Switzerland, 2015, pp. 61–95.

[26] R. Sitko, B. Zawisza, E. Malicka, Graphene as a new sorbent in analytical chemistry, TrAC Trends Anal. Chem., 51 (2013) 33–43.

[27] J. Guerrero-Contreras, F. Caballero-Briones, Graphene oxide powders with different oxidation degree, prepared by synthesis variations of the Hummers method, Mater. Chem. Phys., 153 (2015) 209–220.

[28] K.Y. Yoon, S.J. An, Y. Chen, J.H. Lee, S.L. Bryant, R.S. Ruoff, C. Huh, K.P. Johnston, Graphene oxide nanoplatelet dispersions in concentrated NaCl and stabilization of oil/water emulsions, J. Colloid Interface Sci., 403 (2013) 1–6.

[29] J. Texter, Graphene dispersions, Curr. Opin. Colloid Interface Sci., 19 (2014) 163–174.

[30] J.I. Parades, S. Villar-Rodil, A. Martínez-Alonso, J.M.D. Tascón, Graphene oxide dispersions in organic solvents, Langmuir, 24 (2008) 10560–10564.

[31] S. Lee, Y.-J. Kim, D.-H. Kim, B.-C. Ku, H.-I. Joh, Synthesis and properties of thermally reduced graphene oxide/ polyacrylonitrile composites, J. Phys. Chem. Solids., 73 (2012) 741–743.

[32] H.-I. Joh, H.K. Song, C.-H. Lee, J.-M. Yun, S.M. Jo, S. Lee, S.-I. Na, A.-T. Chien, S. Kumar, Preparation of porous carbon nanofibers derived from graphene oxide/polyacrylonitrile composites as electrochemical electrode materials, Carbon, 70 (2014) 308–312.

[33] K. Goh, L. Setiawan, L. Wei, W. Jiang, R. Wang, Y. Chen, Fabrication of novel functionalized multi-walled carbon nanotube immobilized hollow fiber membranes for enhanced performance in forward osmosis process, J. Membr. Sci., 446 (2013) 244–254.

[34] R. Das, M.E. Ali, S.B.A. Hamid, S. Ramakrishna, Z.Z. Chowdhury, Carbon nanotube membranes for water purification: a bright future in water desalination, Desalination, 336 (2014) 97–109.

[35] B.J. Hinds, N. Chopra, T. Rantell, R. Andrews, V. Gavalas, L.G. Bachas, Aligned multiwalled carbon nanotube membranes, Science, 303 (2004) 62–65.

[36] E. Celik, H. Park, H. Choi, H. Choi, Carbon nanotube blended polyethersulfone membranes for fouling control in water treatment, Water Res, 45 (2011) 274–282.

[37] K.A. Mahmoud, B. Mansoor, A. Mansour, M. Khraisheh, Functional graphene nanosheets: the next generation membranes for water desalination, Desalination, 356 (2015) 208–225.

[38] Y. Han, Z. Xu, C. Gao, Ultrathin graphene nanofiltration membrane for water purification, Adv. Funct. Mater., 23 (2013) 3693–3700.

[39] R.K. Joshi, S. Alwarappan, M. Yoshimura, V. Sahajwalla, Y. Nishina, Graphene oxide: the new membrane material, Appl. Mater. Today, 1 (2015) 1–12.

[40] L. He, L.F. Dumée, C. Feng, L. Velleman, R. Reis, F. She, W. Gao, L. Kong, Promoted water transport across graphene oxide–poly(amide) thin film composite membranes and their antibacterial activity, Desalination, 365 (2015) 126–135.

[41] M.J. Park, S. Phuntsho, T. He, G.M. Nisola, L.D. Tijing, X.-M. Li, G. Chen, W.-J. Chung, H.K. Shon, Graphene oxide incorporated polysulfone substrate for the fabrication of flat-sheet thin-film composite forward osmosis membranes, J. Membr. Sci., 493 (2015) 496–507.

[42] S. Xia, M. Ni, T. Zhu, Y. Zhao, N. Li, Ultrathin graphene oxide nanosheet membranes with various d-spacing assembled using the pressure-assisted filtration method for removing natural organic matter, Desalination, 371 (2015) 78–87.

[43] A.F. Faria, C. Liu, M. Xie, F. Perreault, L.D. Nghiem, J. Ma, M. Elimelech, Thin-film composite forward osmosis membranes functionalized with graphene oxide–silver nanocomposites for biofouling control, J. Membr. Sci., 525 (2017) 146–156.

[44] P.S. Goh, A.F. Ismail, Graphene-based nanomaterial: the state-of-the-art material for cutting edge desalination technology, Desalination, 356 (2015) 115–128.

[45] R.R. Nair, H.A. Wu, P.N. Jayaram, I. V. Grigorieva, A.K. Geim, Unimpeded permeation of water through helium-leak-tight graphene-based membranes, Science, 335 (2012) 442–444.

[46] M. Bhadra, S. Roy, S. Mitra, Desalination across a graphene oxide membrane via direct contact membrane distillation, Desalination, 378 (2016) 37–43.

[47] G. Liu, H. Ye, A. Li, C. Zhu, H. Jiang, Y. Liu, K. Han, Y. Zhou, Graphene oxide for high-efficiency separation membranes: role of electrostatic interactions, Carbon, 110 (2016) 56–61.

[48] Y. Mo, X. Zhao, Y. Shen, Cation-dependent structural instability of graphene oxide membranes and its effect on membrane separation performance, Desalination, 399 (2016) 40–46.

[49] B. Fryczkowska, M. Sieradzka, E. Sarna, R. Fryczkowski, J. Janicki, Influence of a graphene oxide additive and the conditions of membrane formation on the morphology and separative properties of poly(vinylidene fluoride) membranes, J. Appl. Polym. Sci., 132 (2015).

[50] R. Rezaee, S. Nasseri, A.H. Mahvi, R. Nabizadeh, S.A. Mousavi, A. Rashidi, A. Jafari, S. Nazmara, Fabrication and characterization of a polysulfone-graphene oxide nanocomposite membrane for arsenate rejection from water, J. Environ. Heal. Sci. Eng., 13 (2015) 61.

[51] J. Lee, H.-R. Chae, Y.J. Won, K. Lee, C.-H. Lee, H.H. Lee, I.-C. Kim, J. Lee, Graphene oxide nanoplatelets composite membrane with hydrophilic and antifouling properties for wastewater treatment, J. Membr. Sci., 448 (2013) 223–230.

[52] S. Zinadini, A.A. Zinatizadeh, M. Rahimi, V. Vatanpour, H. Zangeneh, Preparation of a novel antifouling mixed matrix PES membrane by embedding graphene oxide nanoplates, J. Membr. Sci., 453 (2014) 292–301.

[53] Y.P. Tang, D.R. Paul, T.S. Chung, Free-standing graphene oxide thin films assembled by a pressurized ultrafiltration method for dehydration of ethanol, J. Membr. Sci., 458 (2014) 199–208.

[54] J. Cong, Y. Chen, J. Luo, X. Liu, Fabrication of graphene/ polyaniline composite multilayer films by electrostatic layer-by-layer assembly, J. Solid State Chem., 218 (2014) 171–177.

[55] K. Cao, Z. Jiang, J. Zhao, C. Zhao, C. Gao, F. Pan, B. Wang, X. Cao, J. Yang, Enhanced water permeation through sodium alginate membranes by incorporating graphene oxides, J. Membr. Sci., 469 (2014) 272–283.

[56] K. Goh, L. Setiawan, L. Wei, R. Si, A.G. Fane, R. Wang, Y. Chen, Graphene oxide as effective selective barriers on a hollow fiber membrane for water treatment process, J. Membr. Sci., 474 (2015) 244–253.

[57] B. Mi, Graphene oxide membranes for ionic and molecular sieving, Science, 343 (2014) 740–742.

[58] M.E. Uddin, R.K. Layek, N.H. Kim, D. Hui, J.H. Lee, Preparation and properties of reduced graphene oxide/polyacrylonitrile nanocomposites using polyvinyl phenol, Composites Part B, 80 (2015) 238–245.

[59] J. Zhu, C. Chen, Y. Lu, J. Zang, M. Jiang, D. Kim, X. Zhang, Highly porous polyacrylonitrile/graphene oxide membrane separator exhibiting excellent anti-self-discharge feature for high-performance lithium–sulfur batteries, Carbon, 101 (2016) 272–280.

[60] J. Zhang, Q. Xue, X. Pan, Y. Jin, W. Lu, D. Ding, Q. Guo, Graphene oxide/polyacrylonitrile fiber hierarchical-structured membrane for ultra-fast microfiltration of oil-water emulsion, Chem. Eng. J., 307 (2017) 643–649.

[61] L. Shen, S. Xiong, Y. Wang, Graphene oxide incorporated thin-film composite membranes for forward osmosis applications, Chem. Eng. Sci., 143 (2016) 194–205.

[62] W.S. Hummers, R.E. Offeman, Preparation of Graphitic Oxide, J. Am. Chem. Soc., 80 (1958) 1339–1339.

[63] B. Zhang, D. Wang, Y. Wu, Z. Wang, T. Wang, J. Qiu, Modification of the desalination property of PAN-based nanofiltration membranes by a preoxidation method, Desalination, 357 (2015) 208–214.

[64] B. Fryczkowska, Z. Piprek, M. Sieradzka, R. Fryczkowski, J.B. Janicki, Preparation and properties of composite PAN/PANI membranes, Int. J. Polym. Sci., 2017 Article ID 3257043, 14 pages (2017).

[65] Y. Feng, G. Han, L. Zhang, S.-B. Chen, T.-S. Chung, M. Weber, C. Staudt, C. Maletzko, Rheology and phase inversion behavior of polyphenylenesulfone (PPSU) and sulfonated PPSU for membrane formation, Polymer, 99 (2016) 72–82.

[66] C. Zhao, X. Xu, J. Chen, F. Yang, Optimization of preparation conditions of poly(vinylidene fluoride)/graphene oxide microfiltration membranes by the Taguchi experimental design, Desalination, 334 (2014) 17–22.

[67] S. Lei, S. Zhong, Y. Wang, Y. Tong, L. Xu, Preparation of monodisperse reduced graphene oxide/polyacrylonitrile composite and its thermal-induced structural transformation, Mater. Lett., 161 (2015) 108–111.

[68] M. Ionita, A. M. Pandele, L. Crica, L. Pilan, Improving the thermal and mechanical properties of polysulfone by incorporation of graphene oxide, Composites Part B, 59 (2014) 133–139.

[69] B.C. Pirlot, I. Willems, A Fonseca, J.B. Nagy, J. Delhalle, Preparation and characterization of carbon nanotube/polyacrylonitrile composites, Adv. Eng. Mater., 4 (2002) 1–11.

[70] R. Fryczkowski, M. Gorczowska, C. Ślusarczyk, B. Fryczkowska, J. Janicki, The possibility of obtaining graphene/polymer composites from graphene oxide by a one step process, Compos. Sci. Technol., 80 (2013) 87–92.